

Elastohydrodynamic friction of robotic and human fingers on soft micropatterned substrates

Yunhu Peng¹, Christopher M. Serfass¹, Anzu Kawazoe², Yitian Shao², Kenneth Gutierrez³, Catherine N. Hill¹, Veronica J. Santos³, Yon Visell² and Lilian C. Hsiao¹

Frictional sliding between patterned surfaces is of fundamental and practical importance in the haptic engineering of soft materials. In emerging applications such as remote surgery and soft robotics, thin fluid films between solid surfaces lead to a multiphysics coupling between solid deformation and fluid dissipation. Here, we report a scaling law that governs the peak friction values of elastohydrodynamic lubrication on patterned surfaces. These peaks, absent in smooth tribopairs, arise due to a separation of length scales in the lubricant flow. The framework is generated by varying the geometry, elasticity and fluid properties of soft tribopairs and measuring the lubricated friction with a triborheometer. The model correctly predicts the elastohydrodynamic lubrication friction of a bioinspired robotic fingertip and human fingers. Its broad applicability can inform the future design of robotic hands or grippers in realistic conditions, and open up new ways of encoding friction into haptic signals.

he goal of haptic engineering is to recreate the perception and experience of touch by applying mechanical forces to skin. Frictional sliding is closely associated with our sense of touch and has been extensively explored in tuning the mechanics of soft materials¹⁻⁴. These advances have inspired robotic hands that capture basic tactile forces, but realistic force feedback remains far from realization⁵. In many applications where a lubricant is present, both surfaces are deformable and the forces depend both on their deformation and the fluid flow. Furthermore, many cases involve contact with deformable patterns with length scales ranging from tens to hundreds of micrometres. The ridges on healthy fingertips represent one such case. Despite the ubiquity of touch, the sliding friction between fingertips and patterned soft surfaces is not fully understood, which makes it challenging to recapitulate the full haptic experience for robots and humans.

Most frictional sliding interactions involve rough surfaces. Such frictional processes are of fundamental interest in physics, as reflected in the research carried out over several centuries. They are also of great practical importance today in diverse areas of industry. However, lubricated sliding on patterned surfaces is not fully understood due to the complex interplay between solid deformation, fluid dissipation and localized flow-directing effects. This so-called elastohydrodynamic lubrication (EHL) regime involves fluid films ('hydrodynamic') that lift and deform the two solid surfaces ('elasto')^{6,7}. Limitations in our understanding of EHL have hampered progress in the design of processes that involve friction, especially in materials and technologies with tunable friction characteristics such as robotic hands and materials with tactile attributes that enable grasping⁸.

Grasp involves the detection of frictional forces to facilitate manipulation⁹ and tactile perception^{10–16}. Thousands of tactile mechanoreceptors in the skin provide the necessary feedback to the nervous system that enables rapid adjustment of grip forces¹⁷. Sliding friction on the skin is greatly affected by lubrication, for example, when sweat or sebum are secreted. More extreme wetting of the skin causes grip force to decrease in a way that is not well

understood¹⁸. Inspired by human grasping abilities, the aim in robotic systems is to design grippers with mechanical attributes, sensors and feedback principles that improve grasp stability. For example, soft surfaces have been used for low-friction manipulation in underwater operations¹⁹. Emerging haptic technologies simulate the feel of natural surfaces by modulating friction through electroadhesion or ultrasonic vibrations^{13,20}. Nevertheless, capturing the feel of realistic surfaces remains challenging because of the difficulty in predicting haptic forces, even with well-characterized surfaces and materials²¹. These challenges become even more pronounced in the presence of EHL. Such types of low-Reynolds-number EHL flows are common in slider bearings and soft tissues^{22,23}. The surface patterns found in these systems appear to alter the dissipation of shear and normal forces in the presence of thin layers of lubricant^{24,25}. Understanding EHL friction is therefore important in fields ranging from manufacturing and telesurgery to touch screens20.

In this study, we generated a physical framework for how the EHL friction on patterned surfaces scales with reduced elasticity and pattern geometry, so as to address the fundamental challenges that hinder the broad application of EHL theory. This framework was first constructed from triborheometry performed on model elastomers and polymers (Fig. 1a,d), and then validated with data from robotic and human fingers (Fig. 1b,c,e,f). The key observation was that patterns with length scales between $10\,\mu\mathrm{m}$ and $100\,\mu\mathrm{m}$ introduce a unique local peak in the EHL friction when they slide against another surface. To understand this effect and to provide a guiding framework for the design of EHL friction, Reynolds lubrication theory was used to model variations in the shear force F_{S} and normal force F_{N} with respect to the sliding speed U and the fluid film thickness h. Statistical analysis showed excellent agreement between the semi-analytical theory, linear regression and all experimental data points.

Lubrication film thickness h for patterned surfaces

Experimental studies have shown that patterned surfaces exhibit EHL tribology that is different from that of flat surfaces^{9,10}, although the differences are not yet fully understood at a mechanistic level.

ARTICLES NATURE MATERIALS

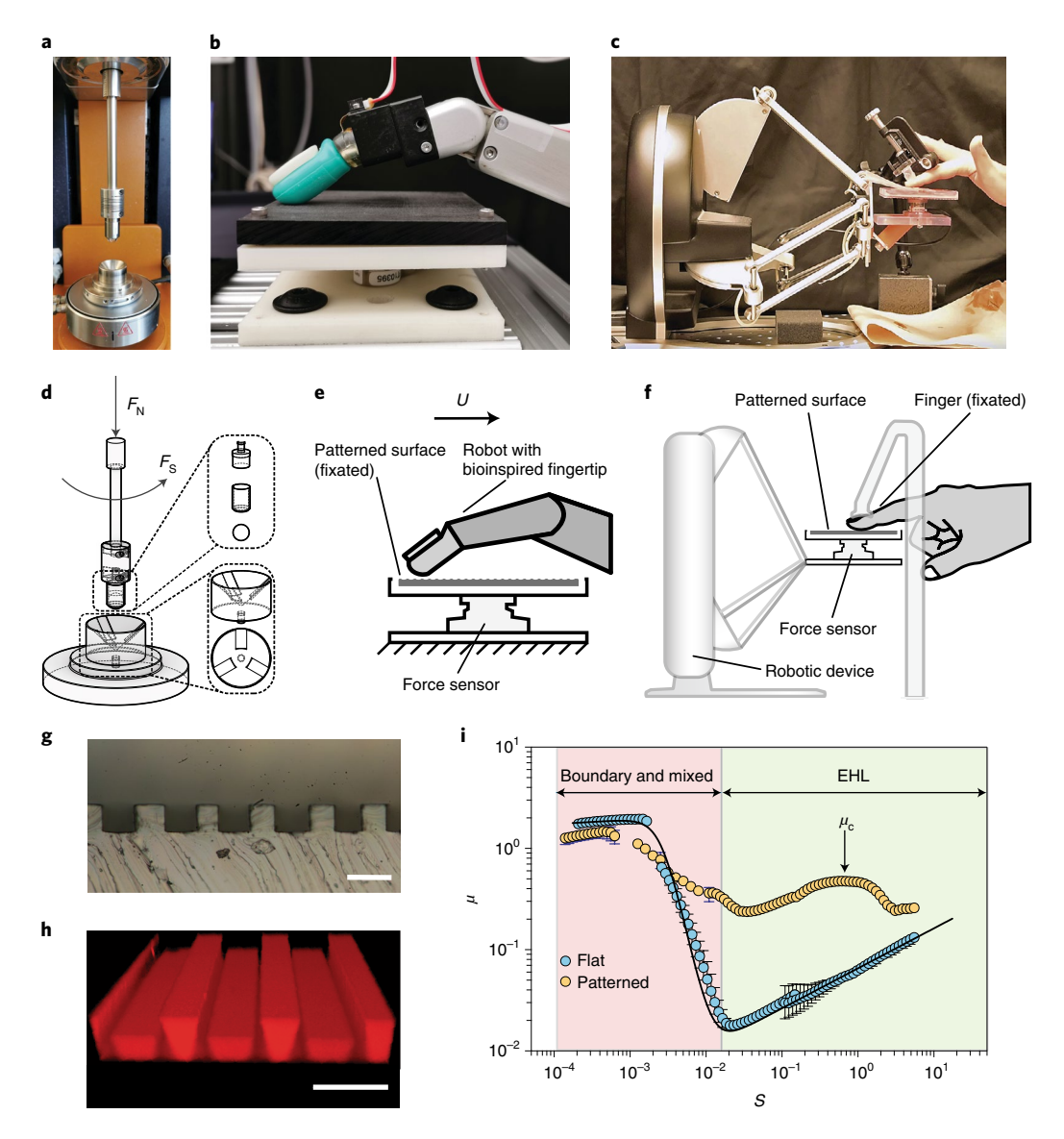


Fig. 1 [Experimental set-ups and Stribeck curves for flat and patterned soft materials. a,d, Photograph (a) and schematic (d) of the ball-on-three-plates triborheological accessory, in which the top ball and three substrates are in three-point contact. The ball rotates and slides against the three bottom substrates at a constant normal force F_N . The friction force F_S is obtained by converting the torque detected at increasing sliding speeds. **b,e**, Photograph (b) and schematic (e) of the lubricated friction between a robotic finger and a patterned surface with a fixated soft substrate. **c,f**, Photograph (c) and schematic (f) of the lubricated friction between a human finger and a patterned soft substrate. The soft substrate on the stage is moved by the robotic device against the fixated human finger. Both sets of haptic experiments were performed in fully flooded EHL conditions. The F_N and F_S values for the haptic experiments were captured by force sensors at the bottom of the sample stages. **g,h**, Optical microscopy (g) and three-dimensional (3D) confocal microscopy (h) images of the patterned soft substrates. Scale bars, 100 μm. **i**, Steady-state sliding friction μ as a function of the Sommerfeld number S for flat and patterned PDMS-PDMS tribopairs with a range of Newtonian lubricants. The solid black line represents an empirical fitting to the Stribeck curve of smooth PDMS-PDMS tribopairs. The pale-red region indicates the boundary and mixed lubrication regime, and the pale-green region indicates the EHL regime where full separation of the surfaces occurs. The error bars indicate the standard deviations from six independent measurements. The Stribeck curve across all S values was obtained using three sets of lubricant viscosities.

The data obtained from chevrons, diamonds and other patterns sliding against human skin suggest that some hexagonal patterns enhance lubricated friction while reducing dry friction during sliding contact²⁶. This gap in knowledge can be traced to the challenges of obtaining analytical solutions in EHL tribology. Grubin²⁷ and Greenwood²⁸ attempted the first analytical descriptions of EHL with reasonable accuracy by assuming that the contact line followed a dry Hertzian contact distribution. Hamrock and Dowson then numerically solved the elasticity and Reynolds equations for macroscopically flat EHL tribopairs lubricated by a piezoviscous

fluid by assuming the pressure is constant in a small element of the contact area²⁹. In doing so, they used dimensional analyses that led to the development of structure—property correlations in tribology. Although modern numerical solutions are able to reproduce the complex conditions within sliding tribopairs, these methods provide less insight into experimental EHL systems, especially when micropatterns are involved. In fact, in their comprehensive review of studies investigating millimetre-sized textures and their frictional effects on slider bearings, Gropper et al. summarized the efforts by stating that 'universal guidelines on texture selection are impossible

NATURE MATERIALS ARTICLES

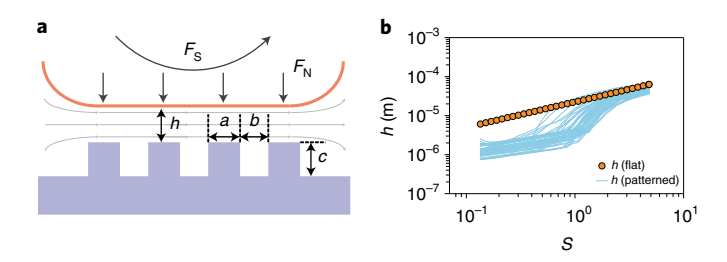


Fig. 2 | EHL lubrication film thickness on patterned surfaces. a, Schematic of the tribopair contact. The solid orange line represents the surface of the top PDMS ball, the solid purple region represents the bottom patterned substrate and the streamlines indicate the direction of lubricant flow. **b**, Fluid film thickness *h* plotted as a function of *S* for patterned soft substrates with each blue curve representing measurements for a distinct surface geometry. The orange circles represent measurements on a flat surface.

to give³³⁰. Our results directly address these scientific and technological challenges by showing that (1) it is quite possible to provide guidelines on texture selection and (2) these guidelines will become powerful tools in the future of haptic engineering.

In our system, h is defined as the distance between the top of the stationary pattern and the bottom of the sliding surface. The Reynolds equations predict that $F_S \sim U/h$ and $F_N \sim U/h^2$. The bulk friction coefficient μ of a tribopair is given by $\mu = F_s/F_N$, where small changes in h generate substantial changes in μ . Although direct measurements of h are possible with specialized birefringence and interferometry^{7,31-33}, the resolution of h measured this way is optically limited to below ~3 µm, even with refractive index-matched materials³⁴, which is less than the film thickness (up to tens of micrometres) generated by many soft tribopairs^{35,36}. Alternatively, mesh-based simulations are used to estimate h for flat tribopairs³⁷. These numerical methods have provided a satisfactory model of μ that matches experimental data in the EHL regime, but are resource-intensive for complex geometries38 and may not fully capture the effect of wall slip³². Instead of using direct measurement techniques, which are not readily available for the sliding forces and velocities of interest in our study³⁹ and are impractical to apply in many cases of interest, we estimated the absolute value of h for patterned tribopairs by combining measurements and correlations. There are three speed-dependent components in the estimated film thickness. The first component, h_a , is the prediction of gap height obtained from Supplementary equation (S8), indicating that the lubricant pressure is concentrated on micropatterns with width a. The second component, $c\varepsilon$, is the change in height of the patterns caused by the fluid's normal load, which generates shear and compression modes. The final component, Δh , is the difference in the gap height measured by the rheometer during sliding with respect to the zero-gap conditions, which are subject to squeeze flow⁴⁰ (Supplementary Fig. 3). Thus, $h = h_a + c\varepsilon + \Delta h$ in our study.

EHL friction on flat and patterned substrates

We used a stress-controlled triborheometer to measure μ and h for 57 patterned substrates spanning four types of materials with different Young's moduli E. The four types of materials were poly(dimethylsiloxane) (PDMS; E=2 MPa), mercaptoester (E=137 MPa), polyester (E=1.2 GPa) and poly(ethylene glycol) diacrylate–alginate double-network (DN) hydrogel (E=3.4 MPa). In our set-up, a soft PDMS ball made a three-point contact with the substrates at a fixed $F_{\rm N}=1.5$ N under all experimental conditions. The patterns consisted of raised stripes with widths $25\,\mu{\rm m} \le a \le 200\,\mu{\rm m}$, valleys with widths $25\,\mu{\rm m} \le b \le 100\,\mu{\rm m}$ and fixed height $c=35\,\mu{\rm m}$ (Figs. 1g,h and 2a). Newtonian lubricants consisting of mixtures of glycerol and water provided the necessary span of viscosities

 $(0.001 \,\mathrm{Pa}\,\mathrm{s} \le \eta \le 1.414 \,\mathrm{Pa}\,\mathrm{s})$ for extracting the full flow curve. Sliding velocities of $500 \,\mu\text{m}\,\text{s}^{-1} \le U \le 35 \,\text{mm}\,\text{s}^{-1}$ were applied to the tribopairs, generating Reynolds numbers of $<3 \times 10^{-3}$. More experimental details on the triborheometry measurements can be found in the Methods section. The data generated by the triborheometer platform were first used to develop the scaling framework before conducting robotic and human finger measurements with lubricants. The dimensionless Sommerfeld number $S = \eta U(R^2/\langle h \rangle)/F_N$ is an independent parameter, where η is the lubricant viscosity and R is the radius of the static contact area (Supplementary Fig. 1). In defining the number S, the value of < h > is fixed for all materials that have the same pattern dimensions. It refers to the average film thickness at which a local maximum in μ is observed for all PDMS-PDMS (P–P) tribopairs (the peak of the patterned EHL curve, denoted μ_c) in Fig. 1i). The point S = 1 demarcates two regimes in EHL in which h scales differently with the sliding speed. The two EHL limits separated by S=1 are discussed in the following section. Similarly, R is defined for all materials using the measured radius for a P-P tribopair having the same patterns. Figure 1i illustrates a representative Stribeck curve obtained from the triborheometer set-up for one of the patterned surfaces, demonstrating that patterns give rise to different frictional behaviour from flat surfaces in the EHL regime. The Stribeck curve is a standard way to characterize the steady-state bulk friction coefficient μ of tribopairs as a function of S.

Scaling framework with two EHL length scales

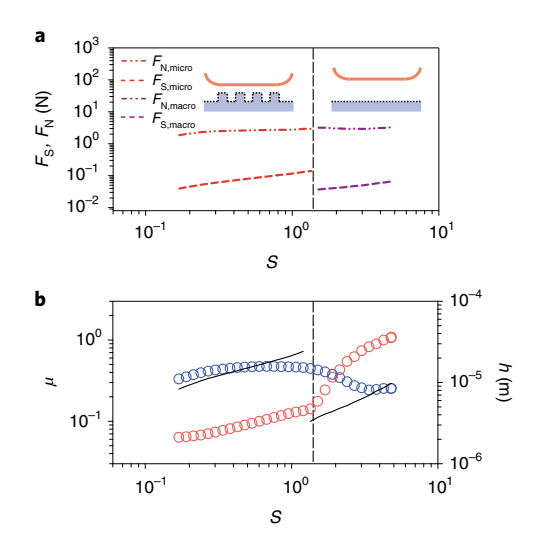
The transition friction coefficient μ_c is identified as the local maximum in μ , observed for patterned geometries but not smooth surfaces (Fig. 1i, EHL regime). Signs of these peaks have previously been observed in scratched stainless-steel-PDMS tribopairs⁴¹ and in fibrillated articular cartilage42. We hypothesize that the presence of μ_c is due to a transition from micro-EHL to macro-EHL, defined as the condition near the point where the lubrication film thickness jumps at intermediate values of S, which is denoted as S_c (Fig. 2b and Supplementary Figs. 4 and 6). The jump in h was only seen for patterned substrates and not for flat ones, and could mechanistically arise from changes in the fluid flow paths at higher S. The observation of two different scalings in h at different values of S led us to consider the length scales and forces responsible for EHL flows (Supplementary Fig. 3). We applied our estimated values of h to solve the Reynolds equations, along with contact area measurements enabled by fluorescent dye transfer (Supplementary Figs. 2 and 7 and Supplementary Tables 3 and 4) to compute μ in the micro- and macro-EHL regimes. The separation of flow regimes using this interpretation gives rise to two lubrication scalings (Fig. 3a). In the micro-EHL regime ($S < S_c$, $h \ll c$), F_S and F_N are given by⁴³

where τ is the shear stress, P is the normal pressure, A_a is the area of the raised patterns and A_b is the area of the valleys. To model the macro-EHL behaviour at $S > S_c$ and h > c, we used

$$F_{\rm N} = PA \sim \frac{\eta URA}{\left(h+c\right)^2} \text{ and } F_{\rm S} = \tau A \sim \frac{\eta UA}{h+c},$$
 (2)

where A is the total contact area measured by the dye transfer method. Because equations (1) and (2) are scaling relations, the scaling prefactors k_{micro} and k_{macro} , which are material property-dependent, were used to generate solutions for each tribopair geometry (Supplementary Fig. 5). The prefactors display a linear dependence on the width a of the raised patterns in the micro-EHL but not in the macro-EHL regime ($k_{\text{micro}} \sim a$ but $k_{\text{macro}} \neq f(a)$). This linear dependence has been previously derived for the pressure gradients

ARTICLES NATURE MATERIALS



a, The predicted friction force (dashed lines) and predicted normal force (dash-dotted lines) as a function of S, separated into the micro-EHL (red) and macro-EHL regimes (purple) by the vertical dashed line. Insets: schematics of the separation of length scales at small and large S. **b**, The experimental data for μ (open blue circles) and h (open red circles) are

Fig. 3 | Modelling the critical EHL transitions for patterned geometries.

schematics of the separation of length scales at small and large S. **b**, The experimental data for μ (open blue circles) and h (open red circles) are plotted as a function of S. The vertical dashed line separates the micro-EHL and macro-EHL regimes. The black solid lines show the predicted EHL friction coefficient. The data in **a** and **b** are representative for a P-P tribopair where $a = 100 \, \mu m$, $b = 100 \, \mu m$ and $c = 35 \, \mu m$.

observed in stepped bearings^{43,44}. The semi-analytical prediction of μ_c can be obtained from equations (1) and (2) at $S=S_c$. Figure 3b shows an example of the model data overlaid on the experimental data for a P-P tribopair ($a=100\,\mu\text{m},\ b=100\,\mu\text{m},\ c=35\,\mu\text{m}$). A number of simplifying assumptions were used to enable the computation of μ_c . The most important assumption was that the compliance of the soft substrate generates a relatively even lubricant gap. Using this method, we were able to model the full EHL tribological phenomena for patterned tribopairs of different materials and geometries (Supplementary Figs. 9 and 10); the semi-analytical theory line showed good agreement with the linear regression fit to the triborheometry data (Supplementary Fig. 8), with a 4.2% difference in the slopes of the lines. Furthermore, a reduced chi-squared χ^2 test conducted for the theory and regression fit⁴⁵ showed an excellent goodness-of-fit ($\chi^2=1.69$, P<0.0005).

Robotic and human haptic friction

The relevance of the EHL scaling law to soft haptics is highlighted in Fig. 4, in which its predictive power is demonstrated using human and robotic fingers. To generate the friction coefficients for the haptic experiments illustrated in Fig. 4, we measured the dynamic shear forces produced by a soft robotic finger sliding on a subset of the patterned substrates (PDMS and polyester) under EHL conditions at speeds and normal forces relevant to wet applications ($F_N = 2 N$, U=5, 15, 30 and 50 mm s⁻¹, $E_{\text{robot}}=0.8 \text{ MPa}$, $0.09 \le S \le 0.9$; Fig. 1b,e, Supplementary Figs. 1 and 11, Supplementary Tables 1 and 2, and Supplementary Video 1; see Methods for details). Separately, we measured the dynamic normal and shear forces produced by three different healthy human fingertips during frictional sliding against the same subset of patterned substrates under fully flooded EHL conditions $(1 \text{ N} \le F_{\text{N}} \le 2 \text{ N}, U = 5, 30, 50, 70 \text{ and } 100 \text{ m s}^{-1},$ $\langle E_{\text{finger}} \rangle = 0.65 \,\text{MPa}$ (ref. 46), $0.36 \leq S \leq 7.2$; Fig. 1c,f, Supplementary Figs. 1 and 12, Supplementary Tables 1 and 2, and Supplementary Video 2; see Methods for details).

Figure 4 shows that the reduced EHL friction coefficient $\widehat{\mu}_c$ falls on a master curve as a function of the pattern geometry (a and b), where $\widehat{\mu}_c = \mu_c E'_{P-P}/E'$ and E' is the conventional reduced modulus of the tribopairs. The friction coefficients measured in the haptic experiments are in excellent agreement with both the scaling law and a linear regression fit to the triborheometer measurements, despite the fact that the contact conditions, sliding velocities and normal forces applied by robotic and human fingers cannot be controlled as precisely. The χ^2 test conducted for the linear regression and data from the robotic and human fingers provided further support for our argument ($\chi^2 = 0.76$, P < 0.0005). Importantly, Fig. 4 reveals that $\widehat{\mu}_c$ values for the soft tribopairs correlate well with the geometry ratio $a/(a+b)^{0.5}$ (see Supplementary Information for details). The correlation between $\widehat{\mu}_c$ and $a/(a+b)^{0.5}$ can be explained by considering the length scale of each repeating unit comprising a stripe and its valley, where the isotropic fluid pressure on an effectively smooth surface is equivalent to the pressure on the top of the patterns at the EHL transition. Combining this length scale with the Reynolds equations captures the observed linear scaling between $\hat{\mu}_{c,exp}$ and $a/(a+b)^{0.5}$.

Outlook

The applicability of this design principle to three different systems opens up many opportunities in which patterns on soft surfaces can be used to alter lubricated friction. EHL friction is dependent on a number of factors, such as wetting, surface geometry, applied pressure and temperature^{23,47}. There is much room for the development of an integrated, experimentally accessible and completely analytical theory based on well-characterized tribological systems. Effective models that identify salient structural and material properties, such as the one presented here, provide a foundation that may be further expanded to irregular textures and rough surfaces. As our findings

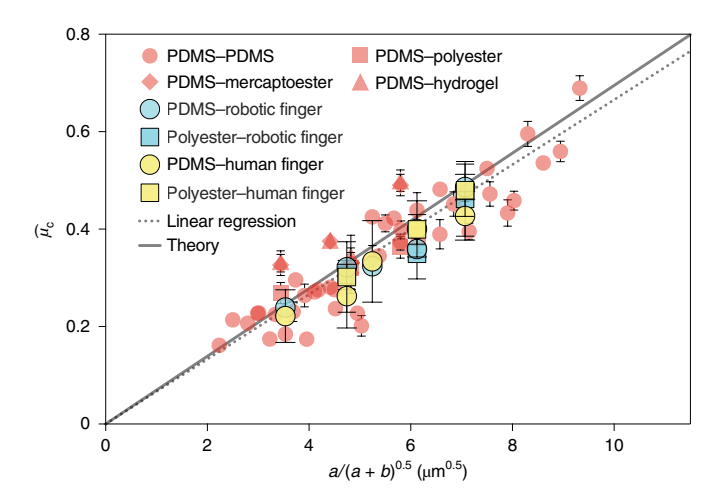


Fig. 4 | Material- and geometry-based framework for the transition **EHL friction coefficient.** The reduced μ_c (defined in Supplementary equation (S19)) from triborheometry, robotic finger sliding and human finger sliding plotted against the geometry parameter $a/(a+b)^{0.5}$. The patterned substrates used in the triborheometry experiments were PDMS, mercaptoester, polyester and DN hydrogel. The error bars for triborheometry experiments represent the standard deviations from six independent samples. For some measurements, the error bar is too small to be visualized. The patterned substrates used in the robotic experiments were PDMS and polyester. The error bars for robotic experiments represent the standard deviations from three independent samples. The patterned substrates used for the human finger experiments were PDMS and polyester. The error bars for human finger experiments represent the standard error from nine independent samples. The linear regression fit and the semi-analytical theory line were obtained from analysis of the triborheometry data.

NATURE MATERIALS ARTICLES

show, the scaling behaviour of tribopairs extends to human and robotic fingers, and elucidates factors affecting friction in grasping and tactile exploration of patterned surfaces. This information is needed for the future design of product surfaces and soft robotic fingers that are better suited to grasping in wet and dirty conditions¹⁹, and may aid the design of algorithms that allow variable-friction touchscreens to reproduce the tactile properties of real surfaces. Our model also holds considerable promise for the design of medical devices that require specific levels of friction at different pressures and velocities^{22,48}. More broadly in the physical science world, EHL friction is important in the bulk mechanics of particulates⁴⁹, in the design of food and cosmetics⁵⁰, and in landscape evolution⁵¹ as they feature deformable tribopairs that slide against one another.

Online content

Any methods, additional references, Nature Research reporting summaries, source data, extended data, supplementary information, acknowledgements, peer review information; details of author contributions and competing interests; and statements of data and code availability are available at https://doi.org/10.1038/s41563-021-00990-9.

Received: 15 September 2019; Accepted: 18 March 2021; Published online: 29 April 2021

References

- Wong, T. S. et al. Bioinspired self-repairing slippery surfaces with pressure-stable omniphobicity. *Nature* 477, 443–447 (2011).
- Bau, O., Poupyrev, I., Israr, A. & Harrison, C. TeslaTouch: electrovibration for touch surfaces. In: *Proc. 23rd Annual ACM Symposium on User Interface Software and Technology* 283–292 (Association for Computing Machinery, 2010).
- Levesque, V. et al. Enhancing physicality in touch interaction with programmable friction. In: Proc. SIGCHI Conference on Human Factors in Computing Systems 2481–2490 (Association for Computing Machinery, 2011).
- Basdogan, C., Giraud, F., Levesque, V. & Choi, S. A review of surface haptics: enabling tactile effects on touch surfaces. *IEEE Trans. Haptics* 13, 450–470 (2020).
- Adams, M. J. et al. Finger pad friction and its role in grip and touch. J. R. Soc. Interface 10, 20120467 (2013).
- Saintyves, B., Jules, T., Salez, T. & Mahadevan, L. Self-sustained lift and low friction via soft lubrication. *Proc. Natl Acad. Sci. USA* 113, 5847–5849 (2016).
- Wang, Y. M., Dhong, C. & Frechette, J. Out-of-contact elastohydrodynamic deformation due to lubrication forces. *Phys. Rev. Lett.* 115, 248302 (2015).
- 8. Dzidek, B., Bochereau, S., Johnson, S. A., Hayward, V. & Adams, M. J. Why pens have rubbery grips. *Proc. Natl Acad. Sci. USA* 114, 10864–10869 (2017).
- Delmas, P., Hao, J. & Rodat-Despoix, L. Molecular mechanisms of mechanotransduction in mammalian sensory neurons. *Nat. Rev. Neurosci.* 12, 139–153 (2011).
- Smith, A. M., Chapman, C. E., Deslandes, M., Langlais, J.-S. & Thibodeau, M.-P. Role of friction and tangential force variation in the subjective scaling of tactile roughness. *Exp. Brain Res.* 144, 211–223 (2002).
- Robles-De-La-Torre, G. & Hayward, V. Force can overcome object geometry in the perception of shape through active touch. *Nature* 412, 445–448 (2001).
- Janko, M., Wiertlewski, M. & Visell, Y. Contact geometry and mechanics predict friction forces during tactile surface exploration. Sci. Rep. 8, 4868 (2018).
- Ayyildiz, M., Scaraggi, M., Sirin, O., Basdogan, C. & Persson, B. N. J. Contact mechanics between the human finger and a touchscreen under electroadhesion. *Proc. Natl Acad. Sci. USA* 115, 12668–12673 (2018).
- Gueorguiev, D., Bochereau, S., Mouraux, A., Hayward, V. & Thonnard, J.-L. Touch uses frictional cues to discriminate flat materials. Sci. Rep. 6, 25553 (2016).
- 15. Weber, A. I. et al. Spatial and temporal codes mediate the tactile perception of natural textures. *Proc. Natl Acad. Sci. USA* 110, 17107–17112 (2013).
- Flanagan, J. R., Burstedt, M. K. & Johansson, R. S. Control of fingertip forces in multidigit manipulation. J. Neurophysiol. 81, 1706–1717 (1999).
- Abraira, V. E. & Ginty, D. D. The sensory neurons of touch. *Neuron* 79, 618–639 (2013).
- Kandaswamy, D., Murthy, M., Alexander, M. & Krothapalli, S. B. Handling objects with very wet skin reduce variability during precision grip task. *Neurosci. Lett.* 703, 177–183 (2019).
- Stuart, H., Wang, S., Khatib, O. & Cutkosky, M. R. The Ocean One hands: an adaptive design for robust marine manipulation. *Int. J. Rob. Res.* 36, 150–166 (2017).

20. Jones, L. Haptics (MIT Press, 2018).

- Khojasteh, B., Janko, M. & Visell, Y. Complexity, rate, and scale in sliding friction dynamics between a finger and textured surface. Sci. Rep. 8, 13710 (2018).
- Greene, G. W. et al. Adaptive mechanically controlled lubrication mechanism found in articular joints. Proc. Natl Acad. Sci. USA 108, 5255–5259 (2011).
- 23. Urueña, J. M. et al. Normal load scaling of friction in gemini hydrogels. *Biotribology* 13, 30–35 (2018).
- Moyle, N. et al. Enhancement of elastohydrodynamic friction by elastic hysteresis in a periodic structure. Soft Matter 16, 1627–1635 (2020).
- Peng, Y., Serfass, C. M., Hill, C. N. & Hsiao, L. C. Bending of soft micropatterns in elastohydrodynamic lubrication tribology. *Exp. Mech.* https://doi.org/10.1007/s11340-021-00715-8 (2021).
- Varenberg, M. & Gorb, S. N. Hexagonal surface micropattern for dry and wet friction. Adv. Mater. 21, 483–486 (2009).
- Grubin, A. Investigation of the Contact Machine Components Ch. 2 (Central Scientific Research Institute for Technology and Mechanical Engineering, 1949).
- 28. Greenwood, J. An extension of the Grubin theory of elastohydrodynamic lubrication. *J. Phys. D* **5**, 2195 (1972).
- Hamrock, B. J. & Dowson, D. Elastohydrodynamic lubrication of elliptical contacts for materials of low elastic modulus I—fully flooded conjunction. J. Lubr. Technol. 100, 236–245 (1978).
- Gropper, D., Wang, L. & Harvey, T. J. Hydrodynamic lubrication of textured surfaces: a review of modeling techniques and key findings. *Tribol. Int.* 94, 509–529 (2016)
- Schilling, J., Sengupta, K., Goennenwein, S., Bausch, A. R. & Sackmann, E. Absolute interfacial distance measurements by dual-wavelength reflection interference contrast microscopy. *Phys. Rev. E* 69, 021901 (2004).
- 32. Davies, H. S. et al. Elastohydrodynamic lift at a soft wall. *Phys. Rev. Lett.* 120, 2–7 (2018)
- Luo, J., Wen, S. & Huang, P. Thin film lubrication. Part I. Study on the transition between EHL and thin film lubrication using a relative optical interference intensity technique. Wear 194, 107–115 (1996).
- 34. Born, M. & Wolf, E. Principles of Optics: Electromagnetic Theory of Propagation, Interference and Diffraction of Light (Elsevier, 2013).
- Fowell, M., Myant, C., Spikes, H. & Kadiric, A. A study of lubricant film thickness in compliant contacts of elastomeric seal materials using a laser induced fluorescence technique. *Tribol. Int.* 80, 76–89 (2014).
- Myant, C., Reddyhoff, T. & Spikes, H. Laser-induced fluorescence for film thickness mapping in pure sliding lubricated, compliant, contacts. *Tribol. Int.* 43, 1960–1969 (2010).
- Lugt, P. M. & Morales-Espejel, G. E. A review of elasto-hydrodynamic lubrication theory. *Tribol. Trans.* 54, 470–496 (2011).
- Scaraggi, M. Lubrication of textured surfaces: a general theory for flow and shear stress factors. Phys. Rev. E 86, 026314 (2012).
- Banquy, X., Burdyńska, J., Lee, D. W., Matyjaszewski, K. & Israelachvili, J. Bioinspired bottle-brush polymer exhibits low friction and Amontons-like behavior. J. Am. Chem. Soc. 136, 6199–6202 (2014).
- Davies, G. A. & Stokes, J. R. On the gap error in parallel plate rheometry that arises from the presence of air when zeroing the gap. *J. Rheol.* 49, 919–922 (2005).
- Scaraggi, M., Carbone, G. & Dini, D. Experimental evidence of micro-EHL lubrication in rough soft contacts. *Tribol. Lett.* 43, 169–174 (2011).
- 42. Bonnevie, E. D. et al. Sub-critical impact inhibits the lubricating mechanisms of articular cartilage. *J. Biomech.* 53, 64–70 (2017).
- Deen, W. M. Analysis of Transport Phenomena 2nd edn (Oxford Univ. Press, 2011).
- Stachowiak, G. & Batchelor, A. W. Engineering Tribology (Butterworth-Heinemann, 2013).
- Taylor, J. Introduction to Error Analysis: The Study of Uncertainties in Physical Measurements (University Science Books, 1996).
- Kalra, A., Lowe, A. & Al-Jumaily, A. Mechanical behaviour of skin: a review. J. Mater. Sci. Eng. 5, 1000254 (2016).
- Bongaerts, J. H. H., Fourtouni, K. & Stokes, J. R. Soft-tribology: lubrication in a compliant PDMS-PDMS contact. *Tribol. Int.* 40, 1531–1542 (2007).
- Seror, J., Zhu, L. Y., Goldberg, R., Day, A. J. & Klein, J. Supramolecular synergy in the boundary lubrication of synovial joints. *Nat. Commun.* 6, 6497 (2015).
- Hsiao, L. C. & Pradeep, S. Experimental synthesis and characterization of rough particles for colloidal and granular rheology. Curr. Opin. Colloid Interface Sci. 43, 94–112 (2019).
- Pradal, C. & Stokes, J. R. Oral tribology: bridging the gap between physical measurements and sensory experience. Curr. Opin. Food Sci. 9, 34–41 (2016).
- 51. Jerolmack, D. J. & Daniels, K. E. Viewing Earth's surface as a soft-matter landscape. *Nat. Rev. Phys.* 1, 716–730 (2019).

Publisher's note Springer Nature remains neutral with regard to jurisdictional claims in published maps and institutional affiliations.

© The Author(s), under exclusive licence to Springer Nature Limited 2021

ARTICLES NATURE MATERIALS

Methods

Fabrication of micropatterned PDMS. The micropatterned silicon wafers (wafer radius R = 76.2 mm) used to generate the model substrates were produced using standard lithographic techniques. The PDMS patterned surfaces were prepared by pouring 12 g Sylgard 184 (Dow Corning) with a ratio of base to curing agent of 10:1 (wt/wt%) onto the wafers and curing at a temperature of 70 °C overnight. The cured substrate has a Young's modulus of 2 MPa and a thickness of 1.9 mm (ref. 52). They were cut into 0.6 cm \times 1.5 cm rectangular slabs for use in tribological characterization. The same curing process was used to fabricate spherical PDMS balls with a radius of 1.27 cm in a custom stainless-steel mould.

Fabrication of micropatterned mercaptoester and polyester. Micropatterned surfaces made from mercaptoesters and polyesters were produced by replica moulding^{53–55}. The elastic moduli for polyester and mercaptoester are 1.2 GPa (ref. 56) and 137 MPa (ref. 57), respectively. Before casting, a micropatterned PDMS mould was created as described previously. Polyester resin (Clear-Lite Casting Resin), styrene monomer and methyl ethyl ketone peroxide (MEKP) catalyst were purchased from TAP Plastics. The mercaptoester used was Norland Optical Adhesive 65 (NOA 65, Norland Products). The resin was mixed with styrene monomer in a 40:1 mass ratio. Following this step, one drop of MEKP catalyst was added for every 4g polyester resin used. The mixture was then mixed and degassed. For the polyester substrates, 12 g resin was poured over the PDMS mould and left at room temperature overnight before being treated at 70 °C for 1 h prior to removal from the mould. The plates for tribological testing were then cut to size using a vertical bandsaw. For the mercaptoester substrates, 12 g NOA 65 was poured over the PDMS mould, covered in aluminium foil and allowed to sit until all the bubbles had dissipated. The NOA 65 was then exposed to ultraviolet (UV) light $(\lambda = 254 \,\mathrm{nm})$ using a Mineralight XX-20S UV Bench Lamp (UVP) for 1 h before being flipped and exposed for another 1 h. The cured NOA 65 was then removed from the mould and plates for tribological testing were cut using a razor blade.

Fabrication of micropatterned DN hydrogel. The micropatterned poly(ethylene glycol) diacrylate (PEGDA) and alginate DN hydrogel substrates were similarly made by replica moulding. To prepare the patterned hydrogel, the PEGDA and alginate monomers were crosslinked in two steps. Alginic acid and PEGDA, obtained from Sigma-Aldrich, were used without further purification. Both alginate and PEGDA were each mixed with deionized water at a concentration of 5 and 40%, respectively. A mixture of the monomers was obtained by mixing the PEGDA and alginate monomer solutions in a 10:1 (wt/wt%) ratio. The photoinitiator 2-hydroxy-2-methylpropiophenone or Darocur (Sigma-Aldrich) was added to the mixture in a ratio of 0.5:99.5 (wt/wt%). The resulting mixture was stirred for 10 min before being transferred to a glass vial. The entire container was covered in aluminium foil and allowed to tumble at 25 r.p.m. for at least 24 h. After 24 h, the sample was placed in a centrifuge at 10,000 r.p.m. for 20 min. The sample was then poured slowly (to prevent the entrapment of bubbles) into the middle of the PDMS mould and placed under UV light for 1 h (λ = 254 nm). Once completely crosslinked, the hydrogel sample was removed from the PDMS mould and soaked in a 1 M calcium chloride solution for 24 h. DN hydrogel plates for tribological testing were cut using a razor blade.

Tribological characterization. The tribology experiments were conducted with a ball-on-three-plates geometry on a stress-controlled rheometer (DHR-2, TA Instruments) at a temperature of 20 °C. The geometry has a ball attached at the top and three plates inserted in the bottom tray (Fig. 1d). The ball was lowered to make contact with the three plates at a fixed normal force of $F_{\rm N}$ = 1.5 N in the presence of a lubricant. The lubricant consisted of a mixture of deionized water and glycerol (Sigma-Aldrich, ≥99.5%). The water–glycerol mixtures were prepared in ratios (wt/wt%) of 0:100, 30:70, 10:90 and 100:0 (η = 0.001, 0.024, 0.768 and 1.412 Pas, respectively). The relative sliding velocity ω between the ball and the plates ranged from 1 to 80 rad s⁻¹.

Because the gap-zeroing procedure used for the tribological measurements was different from traditional rheometry experiments, we provide a detailed description here to highlight the difference. The top geometry (PDMS ball) was lowered against the bottom substrate until a normal load of 5 N was reached. The ball could not be directly lowered onto the pattern substrate with a fluid lubricant as the lubricant would result in squeeze flow, which would give incorrect zero-gap values, and there would also be a high risk of damaging the soft patterns when the load was applied. Instead, we used a flat substrate with no fluid to zero the gap. Then, we replaced the flat substrate with a patterned substrate and added the lubricant before conducting the experiments.

Sliding friction on a robotic finger. Lubricated friction on a bioinspired robotic finger was captured by sliding a fluid-filled elastomeric tactile sensor (BioTac, SynTouch) on flooded micropatterned soft substrates in a sliding direction orthogonal to the patterns. The BioTac sensor is a multimodal bioinspired sensor comprising a rigid core wrapped in an elastomeric skin and filled with fluid to recreate the compliance of a human fingertip. The sensor was mounted on a seven-degrees-of-freedom (DOF) robotic manipulator (WAM with Barrett Hand, Barrett Technology), which performed the sliding across the substrate. The substrate was attached to the top of a 7.6 cm × 7.6 cm black polycarbonate surface.

We measured the lubricated friction of six PDMS and three polyester patterned surfaces (Supplementary Table 1). The polycarbonate surface was mounted on a 3D-printed component with an embedded six-DOF load cell (Nano 17, ATI Industrial Automation). The robot was programmed to slide against the soft substrate at velocities of 5, 15, 30 and $50\,\mathrm{mm\,s^{-1}}$ (Supplementary Table 2). A friction coefficient was computed for each surface and speed as the ratio of the average tangential force to the average normal force over the time interval in which quasi-steady-state sliding contact occurred. The procedures relating to the analysis of these data are provided in the Supplementary Information.

Sliding friction on human fingers. These experiments were conducted with three healthy human fingers (one female age 30, two males ages 27 and 29) and tribopairs involving six PDMS and three polyester patterned surfaces (Supplementary Table 1) at sliding speeds of 5, 30, 50, 70 and 100 mm s⁻¹. This subset of conditions was common to the tribometer and robotic finger experiments. Three independent measurements were conducted for each tribopair and speed. For each human finger, digit 2 of the right hand was positioned at a fixed location and orientation with a clamp and metal stand through adhesives applied to the fingernail (Fig. 1f). A custom apparatus based on a computer controlled the robotic device (Omega 3, Force Dimension) by applying a lateral sliding contact between the volar fingertip and the patterned surfaces as the forces were continuously measured. Each patterned surface was mounted with adhesives on a tray coupled to the robot through a six-axis force-torque sensor (Nano17, ATI Industrial Automation). A compliant real-time position control algorithm (sample rate 4,000 Hz) allowed the robot to generate each sliding trajectory at each of the five specified speeds (Supplementary Table 2) and applied a nominal $F_N = 1 \text{ N}$ during sliding. The true normal and shear force measurements were captured by the force-torque sensor for analysis. Sensor measurements were captured with 14 bit resolution and a sample rate of 4,000 Hz using a data acquisition device (USB-6001, National Instruments). A friction coefficient was computed for each surface, finger and speed as the ratio of the average tangential force to the average normal force over the time interval in which quasi-steady-state sliding contact occurred, In total, the three fingers, five speeds, nine surfaces and three measurement trials yielded 405 friction coefficient values. The procedures relating to the analysis of these data are provided in the Supplementary Information.

The sliding friction experiments on human fingers described herein did not need Institutional Review Board approval, because our experiments did not affect living people physically or physiologically, and we did not seek or receive identifiable private information. The hands shown in Fig. 1c and Supplementary Video 2 are those of co-author A. Kawazoe, who has given her consent to publish the image and video.

Data availability

Source data are provided with this paper. All other data that support the results in this study are available from the corresponding author on reasonable request.

Code availability

The MATLAB codes for solving Supplementary equation (S10) are available at https://doi.org/10.6084/m9.figshare.14233238.

References

- Johnston, I. D., McCluskey, D. K., Tan, C. K. L. & Tracey, M. C. Mechanical characterization of bulk Sylgard 184 for microfluidics and microengineering. J. Micromech. Microeng. 24, 035017 (2014).
- Xia, Y. N. et al. Replica molding using polymeric materials: a practical step toward nanomanufacturing. Adv. Mater. 9, 147–149 (1997).
- Xia, Y. N. et al. Complex optical surfaces formed by replica molding against elastomeric masters. Science 273, 347–349 (1996).
- Fiorini, G. S., Jeffries, G. D. M., Lim, D. S. W., Kuyper, C. L. & Chiu, D. T. Fabrication of thermoset polyester microfluidic devices and embossing masters using rapid prototyped polydimethylsiloxane molds. *Lab Chip* 3, 158–163 (2003).
- Wang, L. & Dandy, D. S. High-throughput inertial focusing of micrometerand sub-micrometer-sized particles separation. Adv. Sci. 4, 1700153 (2017).
- Pinto-Iguanero, B., Olivares-Pérez, A. & Fuentes-Tapia, I. Holographic material film composed by Norland Noa 65^{*} adhesive. *Opt. Mater.* 20, 225–232 (2002).

Acknowledgements

The authors thank R. Ewoldt, J. F. Brady, R. G. Larson, J. Frechette and A. Dunn for discussions. Y.P., C.M.S., C.N.H. and L.C.H. were supported in part by the National Science Foundation (NSF) through award no. CBET-2042635 and the AAAS Marion Milligan Mason Award. K.G. was funded by the Eugene V. Cota-Robles Fellowship from the University of California, Los Angeles. Y.V. was supported by the NSF through award no. 1751348.

Author contributions

Y.P. and L.C.H. designed the study and validated the theory. Y.P., C.M.S. and C.N.H. produced the micropatterned substrates. Y.P., A.K., Y.S. and Y.V. conducted the human

NATURE MATERIALS ARTICLES

finger experiments. Y.P., K.G. and V.J.S. conducted the robotic finger experiments. All authors reviewed the data and wrote the paper.

Competing interests

The authors declare no competing interests.

Additional information

 $\label{lem:supplementary} \textbf{Supplementary information} \ The online version contains supplementary material available at $$https://doi.org/10.1038/s41563-021-00990-9.$

Correspondence and requests for materials should be addressed to L.C.H.

Reprints and permissions information is available at www.nature.com/reprints.